J. Min. Metall. Sect. B-Metall. 55 (2) B (2019) 235 - 251

Journal of Mining and Metallurgy, Section B: Metallurgy

THE EFFECT OF PLATINUM-ALUMINIDE COATING FEATURES ON HIGH-TEMPERATURE FATIGUE LIFE OF NICKEL-BASED SUPERALLOY RENE®80

M.M. Barjesteh [a], K. Zangeneh-Madar [a,*], S.M. Abbasi [a], K. Shirvani [b]

[a*] Malek Ashtar University of technology (MUT), Metallic materials research center, Tehran, Iran
[b] Iranian research organization for science and technology (IROST), Department of advanced materials and new energies, Tehran, Iran

(Received 14 December 2018; accepted 25 April 2019)

Abstract

Low cycle fatigue is the most important failure mode in Aviation/Industrial engine rotary turbine parts. In this paper, the influence of Pt-aluminide coating parameters on high temperature low cycle fatigue behavior of superalloy Rene®80 which is used to manufacture turbine blades, has been investigated. For this purpose, initial platinum layers of different thicknesses (2µm and 8µm) were coated on fatigue specimens. Then the aluminizing process was performed with two conditions of low temperature-high activity and high temperature-low activity. The results of microstructure investigations performed by scanning electron microscope and X-ray diffraction phase analysis indicated a three-layer structure for the coating (bi-phase (Ni,Pt)Al+$PtAl_2$, single-phase (Ni,Pt)Al and interdiffusion zone) with different chemical compositions at both thicknesses of the platinum layer and using both aluminizing methods. Also, the results of low cycle fatigue tests at 871 °C, R=0 and strain rate of 2×10^{-3} s^{-1} showed a decline in fatigue properties in coated specimens as compared to uncoated sample, at total strains of 0.4, 0.8, and 1.2%. This reduction was lower in the low temperature-high activity with platinum layer thickness of 2µm, while it was more significant in the high temperature-low activity with the platinum layer thickness of 8µm. The fractography studies on coated and uncoated specimens indicated a mixed mode of ductile and brittle fracture.

Keywords: *Superalloy; Rene®80; platinum-aluminide; Low cycle fatigue;Fractography.*

1. Introduction

As nickel-based superalloy, Rene®80 provides appropriate mechanical properties at elevated temperatures; it has been widely used to manufacture turbine engine blades [1]. In order to enhance corrosion and oxidation resistance of this alloy, its surface is commonly subjected to aluminide diffusion coating [2]. Nowadays, this kind of coatings that are based on an intermetallic β-NiAl compound are modified with such noble metals as platinum [3]. To achieve platinum-aluminide (Pt-aluminide) coatings, aluminum is diffused into a pre-deposited and diffused platinum enriched layer which was applied on the substrate. It should be mentioned that, based on the aluminum content in aluminizing source, the diffusion treatment can be done in two methods of Low Temperature-High Activity (LTHA) and High Temperature-Low Activity (HTLA) [2]. The nature of these two types of diffusion coatings, which accompanies the combination of coating elements with the substrate elements and vice versa, could have a significant effect on the mechanical properties of alloys. HTLA process is a "one step" method, with outward diffusion of Ni to form β-NiAl coating. On the other hand, LTHA process concerns the inward diffusion of aluminum, typically giving rise to a δ-Ni_2Al_3 coating which requires subsequent heat treatment to convert it to β-NiAl, because δ-Ni_2Al_3 is a brittle phase which has lower mechanical property than β-NiAl. The diffusion behavior of coating/substrate elements also plays an effective role on the DBTT (ductile to brittle transition temperature) of the coatings. Depending on the testing temperature which is above or below the DBTT of the coatings, the positive or negative effects of the coatings on the mechanical properties of the alloys are reported. A reduction in Low Cycle Fatigue (LCF) properties of Rene®80 after applying CODEP-B, a plain aluminide coating, at total strains exceeding 1%, and an increase in this property at total strains below 0.8% at 871 °C have been reported by Rahmani and Nategh [4]. Julis *et al.* [5] investigated LCF properties of Al-Si-coated IN713LC superalloy and reported no effect of the coating on the Basquin curve and its positive effect on the Coffin-Manson curve at 800 °C. On the other hand, the positive effect of Al-Si coating on LCF properties of IN713LC has been reported by Mansuri *et al.* [6] at

**Corresponding author: kzangeneh@mut.ac.ir*

DOI:10.2298/JMMB181214029B

900 °C. In the research performed by Yuan *et al.* [7], the effect of the pre-cracks presence in platinum-aluminide diffusion coating on high-cycle fatigue properties of the IN792 alloy was considered, and the results indicated that the coating thickness imposes direct influence on such fatigue properties, so that no effect was observed for coating of up to 50µm in thickness, while a drop in high-cycle fatigue properties was reported at a coating thickness of 70µm.

As can be observed, the effect of coatings on fatigue properties of nickel-based superalloys is somewhat challenging. A review of related researches shows that the effect of platinum-aluminide coating on LCF properties of nickel-based superalloys has been less worked. On the other side, simultaneous effects of the initial platinum layer thickness and aluminizing conditions (HTLA/LTHA) on this kind of properties of superalloys (especially nickel-based superalloy Rene®80) has not been investigated. The evaluation of the mechanical behavior of Pt-aluminide coated Rene®80 plays a significant role in the design and application of this coating for manufacturing gas turbine engine parts. Therefore, in the present study, the influence of significant parameters of platinum-aluminide coating on LCF properties of alloy Rene®80 have been researched.

2. Experimental

The chemical composition (determined by quantometer apparatus) of the nickel-based superalloy Rene®80 (General Electric Company trademark), used as the substrate in this study is listed in Table 1. According to Figure 1, fatigue specimens were manufactured by machining cylindrical bars of 24 mm in diameter and 120 mm in length obtained from investment casting, as per ASTM E606 [8]. Then, in order to ensure the lack of defects in the specimens, non-destructive FPI and X-ray tests ASTM E1417 [9] and E1742 [10] were performed on them, and the results indicated no surficial or internal defects. Solution and first precipitation heat treatment were performed on specimens at 1205°C for 2h and at 1095°C for 4h [11]. After that, an intermediate layer of nickel with a thickness of 1-2µm was applied with the aim of improving the platinum layer adherence on the surface. In order to deposit nickel layer on the surface, electrolyte solution containing 300-450 gr/l of nickel sulphamate ($Ni(SO_3NH_2)_2.4H_2O$) as an initial source for the production of nickel ions, 2-30 gr/l of nickel chloride ($NiCl_2.6H_2O$) to enhance the anode corrosion and a secondary source for the production of nickel ions, 30-45 gr/l of Boric acid (H_3BO_3) as a soluble pH stabilizer and distilled water were used. In this process pure nickel (% 99.99) was used as the anode and the current density varied between 2-15 A/dm^2, the pH of the solution was between 3.5-5.5, and the solvent temperature was controlled to be between 40-60 °C. The nickel layer deposition process was performed for 90s [12]. The platinum was plated using an electrolyte solution containing 14-18 ml of type P salt (di-nitro di-amino platinum), 70-90 g/l sodium carbonate (Na_2CO_3), 40-70 g/l sodium acetate ($NaCH_3COO$) and 1liter of distilled water at 90°C under a current density of 0.2-0.4 A/dm^2 and electrolyte pH of about 10.5 [13]. In order to achieve a platinum layer with a thickness of either 2µm or 8µm, different times (150 and 480 min) were considered for the plating process. Heat treatment at 1050°C for 2h was applied on the platinum layer to enhance the adhesion and improve the platinum distribution in the substrate, followed by cooling the specimens in the furnace at 400°C and then air-cooled [11,13]. The aluminizing process was performed under two conditions, namely low temperature-high activity (LTHA, at 750°C for 4h [14] and after that post aluminizing at 1050ºC for 2h) and high temperature-low activity (HTLA, 1050°C for 2h) via powder cementation. The compositions of the cementation powders used for LTHA and HTLA were selected as $2NH_4Cl$-12Al-$86Al_2O_3$ wt. %) and $1NH_4Cl$-4Al-$95Al_2O_3$, respectively. After the formation of the platinum-aluminide coating on the surface, an aging treatment was carried out at 845ºC for 16h [11]. Figure 2 shows the work flow of the coating process. Microstructural studies were conducted using a Scanning Electron Microscope (SEM) equipped with Energy Dispersive Spectroscopy (EDS) both prior to fatigue test (to ensure the quality of the coatings) and after the test (to investigate fracture surfaces) according to ASTM E3 [15], and ASTM E883 [16].

X-ray diffraction analysis was also performed

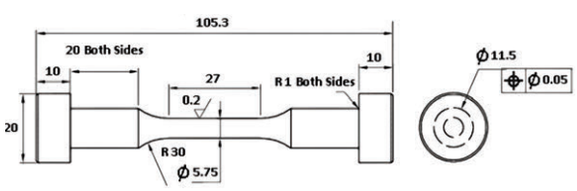

Figure 1. *Dimensions (mm) of the standard fatigue test specimen according to ASTM E606 [8]*

Table 1*. Chemical composition of nickel-based superalloy Rene®80 used in this study (wt. %)*

C	Cr	Co	Mo	W	Al	Ti	Fe	Zr	V	B	Si	Mn	Ni
0.16	13.81	9.69	4.23	4.02	3.02	4.87	0.12	0.05	0.05	0.02	0.02	0.03	Bal.

using an XRD apparatus (Inel Equinox 6000 with X'Pert High Score Plus v2.0, Cu Kα1 with a graphite monochromator, 2θ = 16° to 93°, 40Kv, 37mA) to determine the distributions of different phases across the thickness of the coatings and measure residual stresses. Micro-hardness test was performed perpendicular on the platinum-aluminide coatings and the substrate under an applied force of 50gf, based on ASTM E384 [17] by use of automatic Akashi micro-hardness set equipped with Clemex Software.

The tensile test was performed on the coated and uncoated specimens at 871°C and strain rate of 1.6×10^{-4} s^{-1} using a Universal ATM apparatus equipped with an electrical furnace that could apply temperatures up to 1000°C, in accordance with ASTM E21 [18].

The coated and uncoated specimens were subjected to LCF test at 871°C according to ASTM E606 [8] at total strains ($(\Delta\varepsilon_t\ (\%) = \Delta\varepsilon_P + \Delta\varepsilon_e)$ of %0.4, %0.8, and %1.2 at a strain rate of 2×10^{-3} s^{-1}, tensile-tensile, triangular wave and $R = \varepsilon_{min}/\varepsilon_{max} = 0$ utilizing an Instron apparatus equipped with an electrical furnace at 1000±1°C.

3. Results and discussion

3.1. Microstructure characterization of the coatings

Before the investigation of the platinum-aluminide coatings, the substrate microstructure (Fig. 3) and hardness were researched. As shown in this figure, the application of coatings in both conditions of LTHA and HTLA has no effect on the substrate microstructure. Figure 3 also shows fixed γ′ ($Ni_3(Al,Ti)$) phase (this compound is the strengthening phase of alloy) under the above mentioned conditions, so that the area percentage of this phase was determined to be about 38±4% by using image analyzer software. The hardness of the substrate after

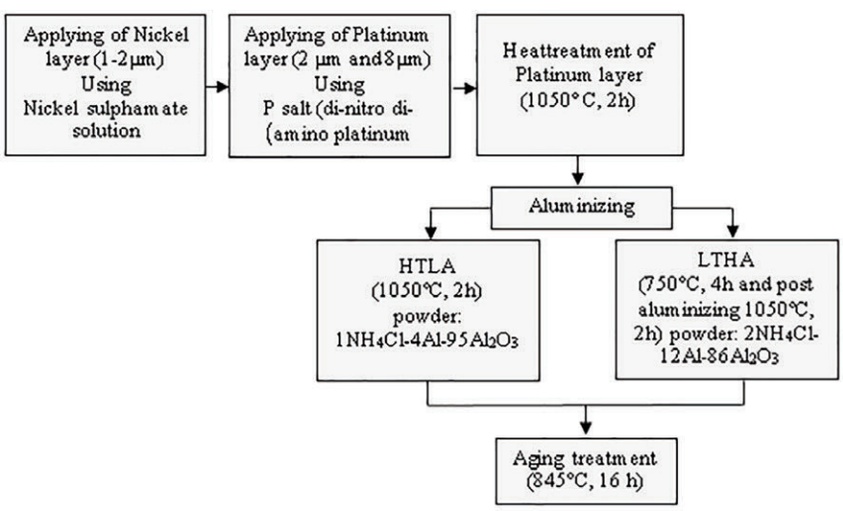

Figure 2. *Work flow of the coating processes*

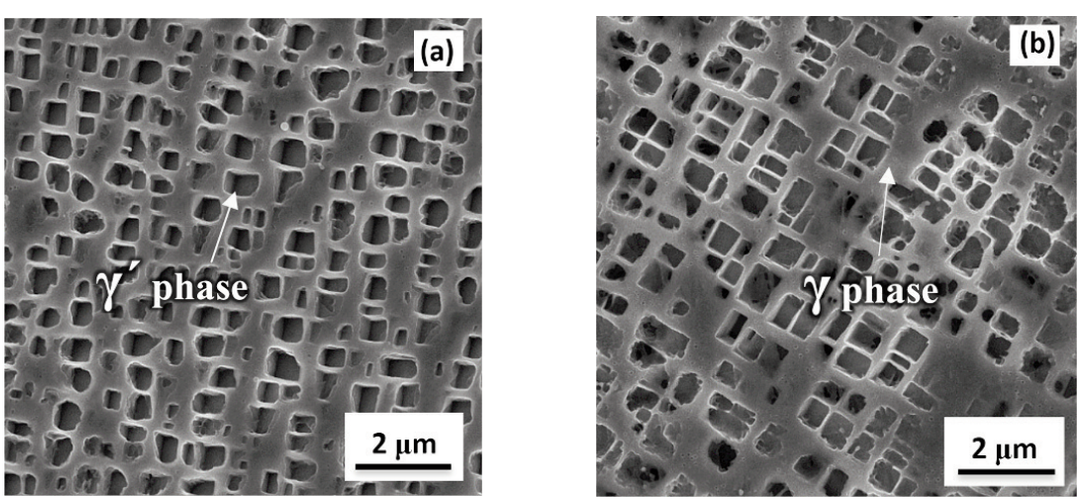

Figure 3. *The SEM images of the γ' phase changes after aluminizing by the methods of a) LTHA, and b) HTLA*

HTLA and LTHA processes was measured as 406 and 410 Vickers, respectively (three points were measured and the average value was reported).

Figure 4 shows the microstructure of the platinum-aluminide coatings under HTLA and LTHA for different thicknesses of the initial platinum layer. As can be observed, in both aluminizing conditions, the microstructure of the coatings in the outer layer was composed of bi-phase: ξ-$PtAl_2$ and β-(Ni,Pt)Al. The next layers of the coatings included β-(Ni,Pt)Al (the single-phase intermediate layer), and IDZ (interdiffusion zone-the final layer of the coating-metal interface).

In order to determine the phases in the coatings, particularly the ξ-$PtAl_2$ phase, and also ensure the transition of the brittle phase of Ni_2Al_3 to the ductile phase of β-NiAl in LTHA, X-ray diffraction analysis was performed on the specimens, with its results shown in Figure 5. According to this figure, $PtAl_2$ and NiAl phases were identified in the coatings.

The results of the platinum-aluminide coatings thickness measurements by SEM indicated that with increasing the initial thickness of platinum from 2µm to 8µm under HTLA, the final coatings thickness increased from 92 µm to 102µm. The corresponding final coating thicknesses to the LTHA were 128µm and 148 µm, respectively. As can be seen from the figures, an increase in the thickness of the platinum layer improved the thickness of the external ξ + β layer for both HTLA and LTHA. Due to the high level of aluminum under LTHA, the thickness of the intermediate β-(Ni,Pt)Al layer is higher than that under HTLA, which is in accordance with Das study results [19]. The thickness of IDZ layer (which is the place for accumulation of refractory elements such as tungsten, titanium, chromium, molybdenum, and cobalt) was also reported to be lower in LTHA as compared to HTLA.

The variation in thickness of the platinum-aluminide coating for different initial platinum thicknesses in HTLA and LTHA methods is listed in Table 2. (Three sections are measured and reported with accuracy ±4µm for the outer layer, ±7µm for the middle layer and ±1µm for IDZ).

Chromium is one of the most important elements contributing to the formation of TCP phases [20], the

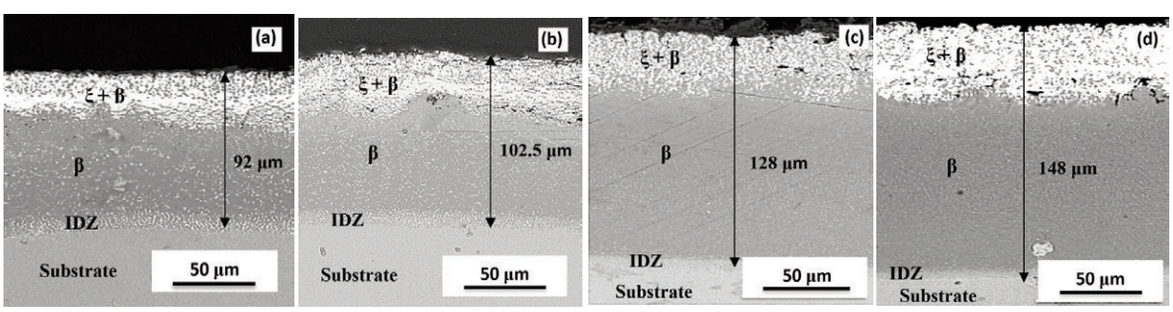

Figure 4 *SEM images of the platinum-aluminide coating under HTLA for an initial thickness of platinum (a) 2µm and (b) 8µm, and also under LTHA for an initial thickness of platinum (c) 2µm and (d) 8µm. (ξ: $PtAl_2$, β: (Ni, Pt) Al)*

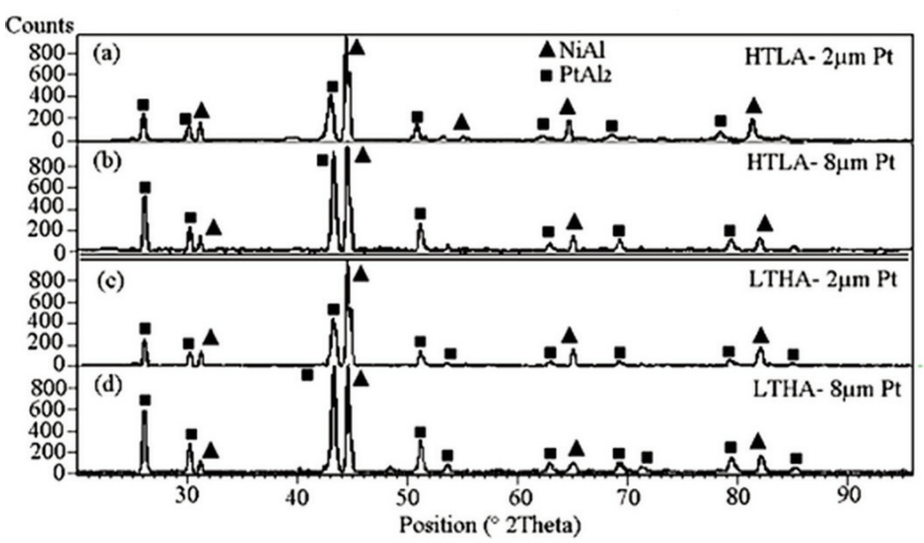

Figure 5. *Results of XRD analysis on platinum layers of (a) 2µm and (b) 8µm in thickness under HTLA condition, and those of (c) 2µm and (d) 8µm in thickness under LTHA condition*

distribution of this element in the two aluminizing conditions was investigated using EDS line scan analysis at a magnification of 750x, with the results presented in Figure 6. As shown in this Figure, the chromium content in the IDZ layer of HTLA was higher. Indeed, due to the higher thickness of the β layer in LTHA, more chromium content was dissolved in this layer that resulted in less Cr in the IDZ.

Figure 7 demonstrates the variations of the concentration of nickel, platinum, and aluminum in the perpendicular direction of the coatings at different thicknesses of the platinum layer under the two aluminizing conditions.

The results of this analysis are indicative of the internal diffusion of platinum and aluminum and external diffusion of nickel. The diffusion depth and concentration slope of platinum are affected by the initial thickness of the platinum layers, so the amount of platinum diffusing increases with increasing the initial platinum layers thickness under both LTHA and HTLA.

3.2. Low cycle fatigue behavior (LCF Life)

3.2.1. Monotonic stress-strain behavior

Before proceeding to the determination of the coatings effect on LCF life of Rene®80 (cyclic stress-strain behavior) to obtain an appropriate understanding of the cyclic hardening or softening

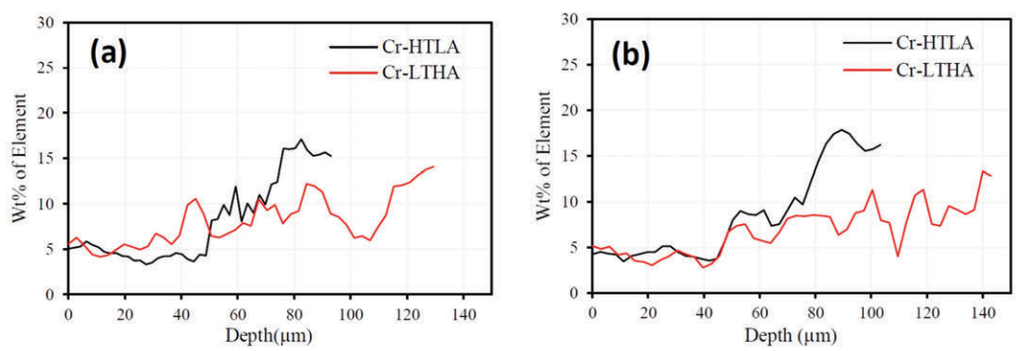

Figure 6. *Comparison of variations of the chromium content across coatings created under LTHA/HLTA for platinum layer thicknesses of (a) 2μm and (b)* 8μm

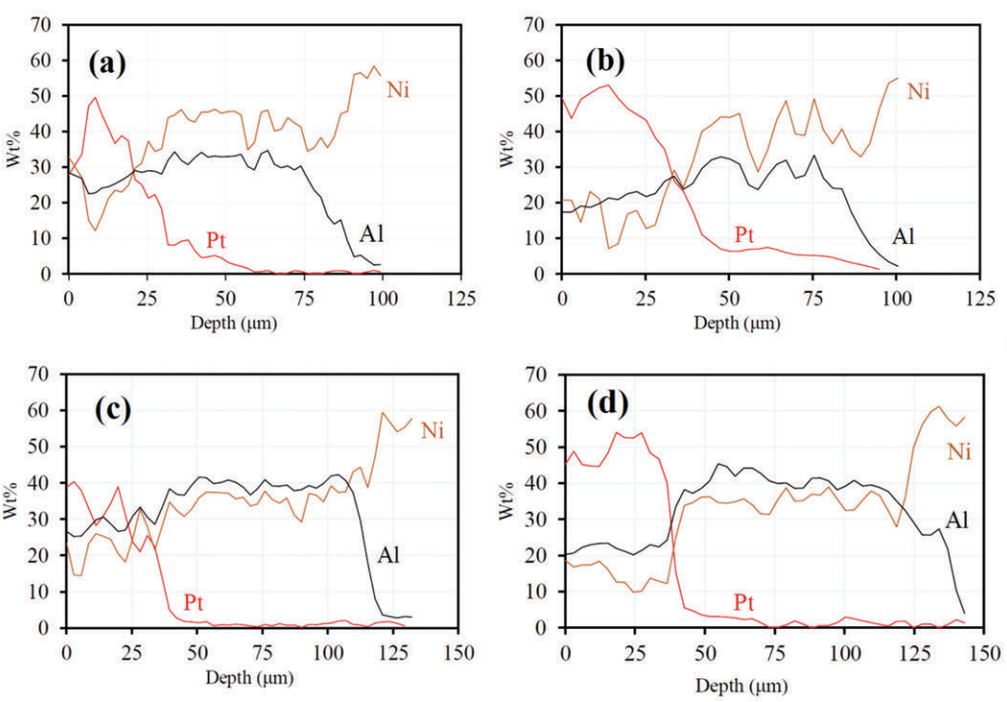

Figure 7. *Variations of concentration and diffusion depth of platinum, aluminum, and nickel under HTLA with an initial platinum layer of (a) 2μm and (b) 8μm in thickness, and (c) 2μm and (d) 8μm initial platinum layer under LTHA*

***Table 2**. Thickness of platinum-aluminide layers as a function of initial platinum layer thickness for two aluminizing methods: HTLA and LTHA*

Thickness of platinum layer (μm)	2			8		
	β+ξ	β	IDZ	β+ξ	β	IDZ
HTLA	32	51	9	47	42	13.5
LTHA	39	84.5	4.5	45	97	4

behavior of the alloy (to be discussed later on), a tensile test (monotonic stress-strain behavior) was performed at 871 on the uncoated (after heat treatment according to AMS5403 [11]) and coated specimens. The results are reported in Tables 3 and 4. It is mentioned that, under each set of conditions, the tensile and fatigue tests were performed on two specimens.

3.2.2. Cyclic stress-strain behavior of uncoated specimens.

The results of the fatigue test on the uncoated specimens are reported in Table 5, where $\Delta\varepsilon_t$ is total strain amplitude, σ_{max} is maximum cyclic stress, σ_{min} is minimum cyclic stress, N_i is the number of cycles by which the first drop in the alloy properties is observed (crack nucleation), and N_f is the number of cycles to fracture.

The results of LCF test on the uncoated specimens of alloy Rene®80 in the form of strain vs. stress hysteresis loops are shown in Figure 8. The hysteresis loops indicate changes in the resistance behavior of the material against deformation under cyclic loading. If the material is subjected to a constant controlled strain cycle, the material behavior under the effect of the load includes cyclically harden or soften, steady state, or a combination of all of them. In the cyclic hardening mode, with increasing the number of successful cycles (in the first several cycles), the stress increased accordingly, while in the cycling softening mode, the opposite occurred. In both modes, the value of stress decreased gradually to reach a steady state. As can be seen from the diagrams plotted in Figure 8, the alloy Rene®80 showed a cyclic softening behavior at R=0. Generally in the alloy, if $S_u / S_y < 1.2$ (where S_u is ultimate strength and S_y is yield strength), the alloy will exhibit cyclic softening behavior, and if $S_u/S_y > 1.4$, the alloy will exhibit cyclic hardening behavior [21]. Tensile test results (Tables 3 and 4) show that the condition of $S_u / S_y < 1.2$ is true for all cases.

Figure 9 shows variations of maximum, minimum stresses and the stress range ($\Delta\sigma = \sigma_{max} - \sigma_{min}$) as functions of time for uncoated specimens at different total strains.

As is evident in these plots and hysteresis loops, the first cycle exhibits a large total stress. In this case, the specimen undergoes deformation until total strain, followed by complete unloading. Then, the stress level reaches a steady state, and after successive cycles at time t_i (the N_i cycle) and with the creation of

***Table 3.** Results of tensile test on alloy Rene®80 (uncoated) at 871°C*

Tensile Properties	(MPa)UTS	(MPa)YS	% El	% RA
AMS 5403 (Min)	620	415	---	15
Sample1	706	595	9	16.5
Sample2	696	585	7	15.5

***Table 5.** Results of LCF test on uncoated Rene®80 specimens (T = 871°C, R =0, $\dot{\varepsilon}$ = 2 × 10^{-3} s^{-1})*

$\Delta\varepsilon_t$ (%)	σ_{max} (MPa)	σ_{min} (MPa)	N_i	N_f
0.4	712.78	-484.5	1600	1909
	710.27	-475.2	1588	1892
0.8	742.5	-532	422	487
	757	-550.4	425	474
1.2	819.8	-612.3	141	152
	835.3	-607.3	133	139

***Table 4.** Results of the tensile test on the coated specimens with different thickness of initial platinum under different aluminizing conditions at 871°C*

Aluminizing Process	HTLA				LTHA			
Thickness of Pt (μm)	2		8		2		8	
	Sample1	Sample2	Sample1	Sample2	Sample1	Sample2	Sample1	Sample2
UTS (MPa)	672	658	504	492	677	663	614	602
YS (MPa)	569	561	472	462	583	573	541	531
%El	6	6	5	4.5	7.5	7.5	6.5	6.5
%RA	12.5	11.5	10.5	9.5	16	15	14.5	13.5

the first crack, suddenly the stress level drops and the specimen fails after a limited number of cycles at time t_f (the N_f cycle). Rahmani and Nategh [22] reported that at the first cycle, initially, slip systems become active in the perpendicular direction to the cyclic stresses, and dislocations are concentrated in the γ matrix phase due to its lower strength compared to the precipitation γ′ phase. Subsequently, the interactions between matrix dislocations and the precipitation γ′ phase give rise to a hexagonal (i.e. honeycomb) network which reduces the elastic energy of the entire system while decreasing and releasing some stress during the loading. As the number of cycle increases, the deformations become homogeneous and more slip systems become active, and as a result, the density of dislocations is increased. Upon dislocation-dislocation interactions, the strength of the superalloy decreases and the specimen is failed at the N_f cycle. With further increasing the applied strain, the distribution of the matrix dislocations becomes more homogeneous, with their density enhanced. This makes it possible for the dislocations to shear particles of γ′, and upon arriving the dislocations into this phase, the coherency between the γ and γ′ decreases. Finally, the specimen will yield within a shorter time [22].

3.2.3. Cyclic stress-strain behavior of coated specimens

The results of the fatigue tests on the coated specimens under HTLA and LTHA are presented in Table 6.

The results indicate a reduction in the fatigue life of the coated specimens under both LTHA and HTLA, as compared to the uncoated specimen (Table 5).

However, the reduction was more significant under HTLA. Moreover, an increase in the initial thickness of platinum was associated with the reduced fatigue life. With an initial platinum thickness of 2μm at the total strain of 0.4% under HTLA, the number of cycles tolerated by the specimens up to failure (N_f) was 1791 cycles, while the corresponding number to LTHA was 1841 cycles. The uncoated specimen tolerated 1909 cycles to fail, indicating 6% and 3.5% decrease in the number of tolerated cycles by the coated specimens, respectively, as compared to the uncoated specimen at the same total strain. The reduction in the number of tolerated cycles for the platinum thickness of 8μm at the same total strain under HTLA and LTHA was reported to be 26% and 15%, respectively. In Figures 10 to 13, for demonstration purposes, hysteresis loops and variations of stress with time for coated specimens

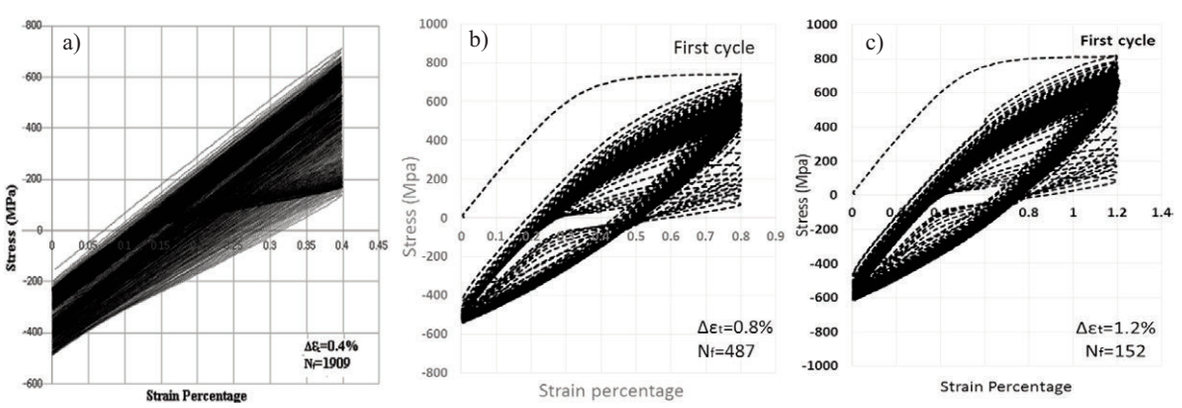

Figure 8. *Stress-strain hysteresis loops for uncoated specimens at different total strains at 871°C for total strains of (a) 0.4%, (b) 0.8%, and (c) 1.2%.)*

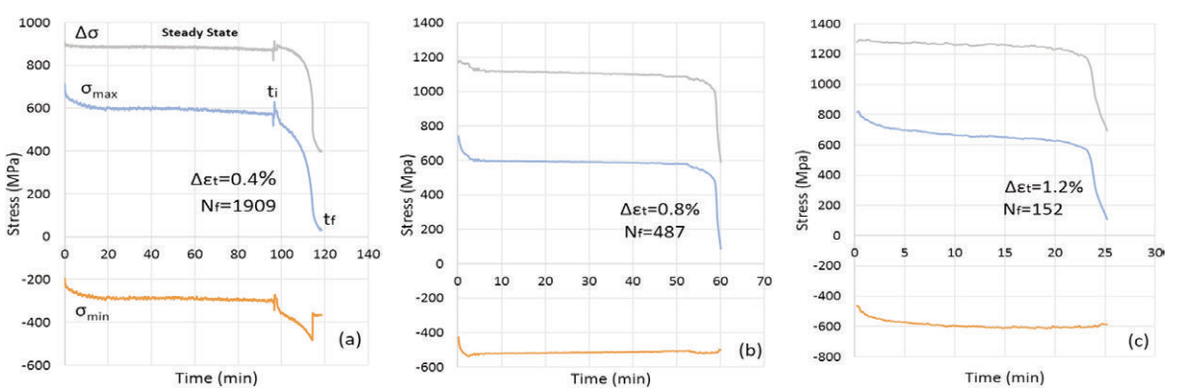

Figure 9. *Variations of maximum and minimum stresses with time for uncoated specimens at 871°C for total strains of (a) 0.4%, (b) 0.8%, and (c) 1.2%*

under HTLA and LTHA with platinum of 2μm and 8μm in thickness at the total strain of 0.8% are shown.

As is evident from the figures, the fatigue behavior of all of the coated specimens resembled those of the uncoated specimen, i.e., showing a cyclic softening behavior. Also, it is evident that the maximum test time (about 115 min, i.e. 1841 cycles) for the coated specimens was related to the coated specimen with 2μm of platinum under LTHA at a total strain of 0.4%. During the test, this specimen showed only 3.5% lower fatigue life compared to the uncoated specimen. The lowest duration was related to the coated specimen with 8μm of platinum under HTLA at a total strain of 1.2%, where the specimen failed following a limited time of 13 minutes (61 cycles), showing 59.5% decrease in fatigue life, as compared to the

Table 6. *The LCF test results on coated specimens of Rene®80 with platinum layers of 2μm and 8μm in thickness under HTLA and LTHA. ($T = 871^oC$, $R = 0$, $\dot{\varepsilon} = 2 \times 10^{-3}\ s^{-1}$)*

Thickness of Pt (μm)		$\Delta\varepsilon_t$ (%)	σ_{max} (MPa)	σ_{min} (MPa)	N_i	N_f
2	HTLA	0.4	710.1	-506.57	1547	1791
			712.14	-510.1	1531	1782
		0.8	781.9	-550.8	420	460
			782.8	-551.4	414	452
		1.2	846.1	-657.3	109	118
			842.1	-651.9	95	105
			857.2	-692.4	62	76
8		0.4	711.61	-326.22	1386	1415
			722.48	-339.04	1374	1395
		0.8	827.6	-542.5	295	316
			823.6	-551.2	270	301
		1.2	860.6	-638.6	46	61
			864.4	-671.3	31	54
2	LTHA	0.4	697.1	-513.44	1590	1841
			705	-521.14	1579	1796
		0.8	763.4	-555	429	472
			759.2	-534	422	465
		1.2	836.2	-639.6	109	132
			841.9	-740.2	102	121
8		0.4	702.28	-463.8	1555	1607
			706.48	-469.04	1517	1592
		0.8	814.3	-546.8	369	381
			808.3	-506.7	373	377
		1.2	853.6	-699.6	62	83
			857.1	-670.7	54	73

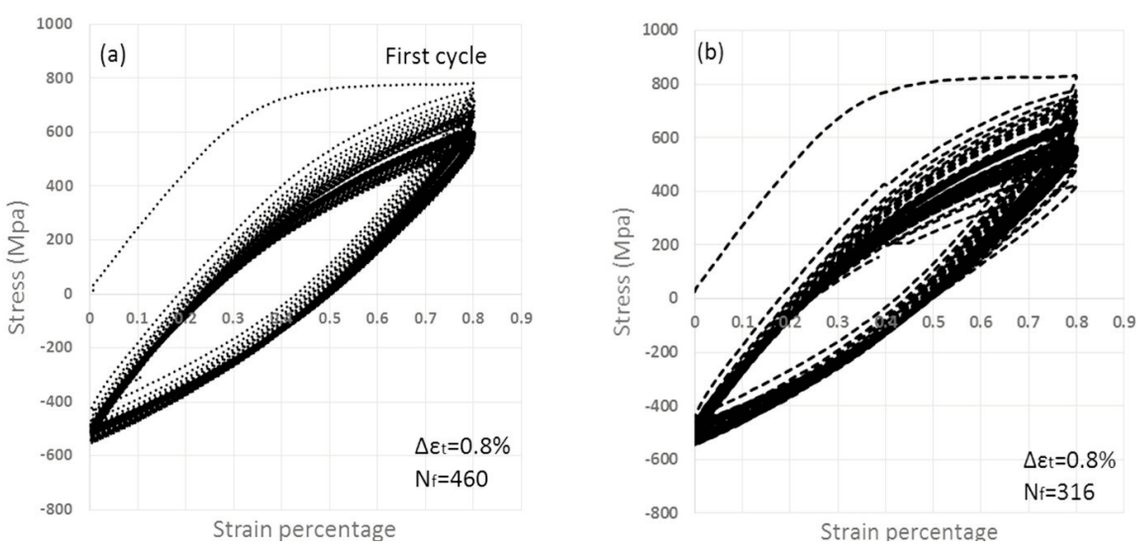

Figure 10. *Hysteresis stress-strain loops for coated specimens under HTLA condition at total strain of 0.8%, temperature of 871°C, and initial platinum layer thicknesses of (a) 2μm, and (b) 8μm*

uncoated specimen. An important cause supporting the reduction of fatigue strength in these specimens is the low ductility of this specimen. Fatigue crack nucleation is controlled by plastic deformation, and the cracks tend to develop and grow within regions of lower ductility. Therefore, higher alloy ductility increases the fatigue life of the alloy in a given range of applied strain. As is seen from the tensile test results (Tables 3 and 4), the best ductility was that of the uncoated specimen while the worst ductility was that of this specimen. On the other hand, as a failure strain of aluminide coatings is generally low, the failure critical stress of such coatings would be low as well [23]. When the fatigue test is run on coated specimens, considering the high level of the stress applied at the first cycle, a crack was nucleated in the coating during early cycles, and grew rapidly toward the substrate-coating interface. Subsequently, stress concentration will develop around the end of the crack in the coatings. Stress intensity at the crack tip can be calculated using $K_I=Y\times\sigma\times\sqrt{a}$ [23], where Y depends on the crack geometry and loading conditions, σ is the applied stress, and a is the crack length. Since the crack grows within the coating rapidly, one can assume the crack length as being equal to its thickness. The relationship indicates that, if the value of crack length is sufficiently large, the value of K_I will exceed the value of ΔK_{th} (critical stress concentration intensity of the alloy), making the crack grow rapidly into the substrate, and leading to its

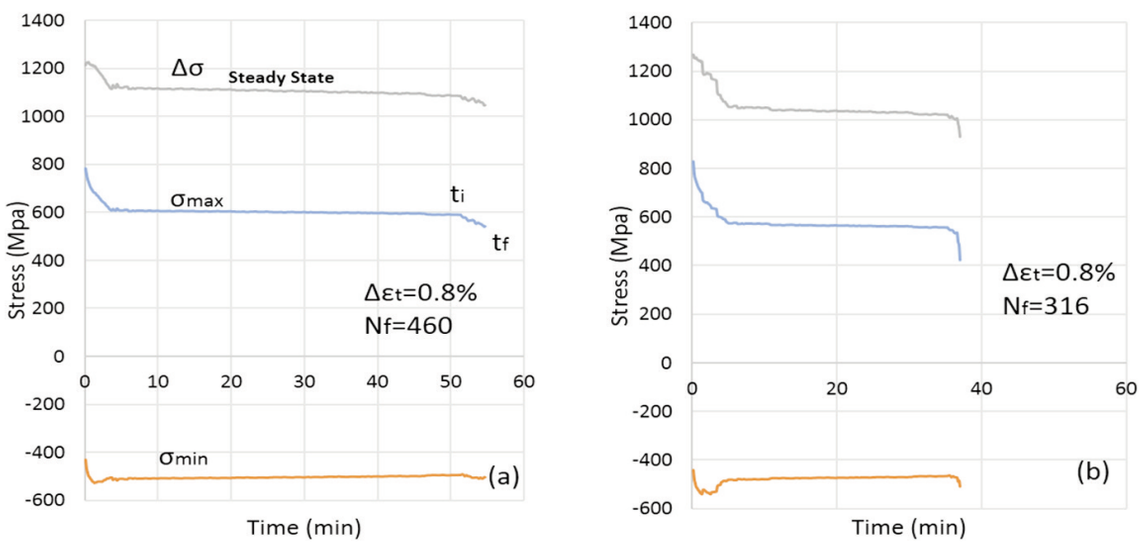

Figure 11. *Variations of maximum and minimum stresses with time for coated specimens under HTLA condition at total strain of 0.8%, temperature of 871°C, and initial platinum layer thicknesses of (a) 2μm, and (b) 8μm*

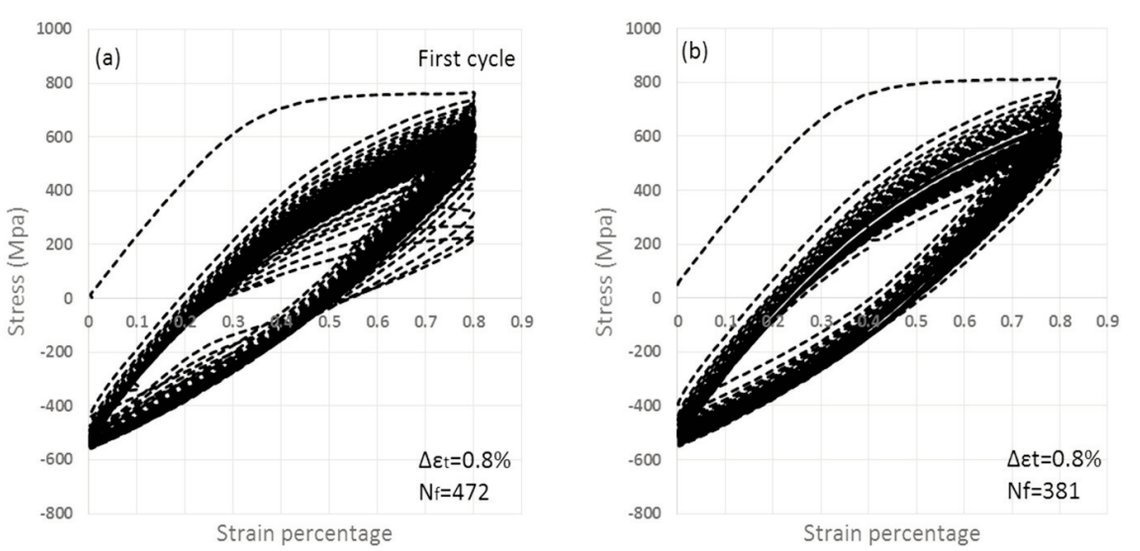

Figure 12. *Hysteresis stress-strain loops for coated specimens under LTHA condition at total strain of 0.8%, temperature of 871°C, and initial platinum layer thicknesses of (a) 2μm, and (b) 8μm*

failure. So, an increase in the coating thickness under both HTLA and LTHA resulted in a reduction in the fatigue life of the alloy.

Another reason behind the decrease in the fatigue life of the coated specimens is related to the DBTT. According to this relationship ($T_{DBTT} = 698 + 10t_{Pt}$) [24], where T_{DBTT} is ductile-to-brittle temperature (ºC) and t_{Pt} represents platinum layer thickness, an increase in platinum thickness directly affects the increase in this parameter. At temperatures lower than DBTT, the properties of the coating are highly different from the base alloy, whereas, in the temperature range above DBTT, the differences between the properties of the metal coatings and the base are lower [4]. Therefore, the working temperature of coated Rene®80 should be chosen in a way that the properties of its coating remain in the ductile range [25].

3.2.4. Fatigue behavior of coated samples in HTLA and LTHA

In the present research, with increasing the thickness of the coatings under either of the LTHA and HTLA, the fatigue life degraded, but under the LTHA, despite the increase in the coatings thickness as compared with HTLA, less significant reduction on the fatigue life was observed, with its reason being possibly related to factors such as coatings composition stoichiometry, mechanism of elemental diffusion into the coatings and substrate, ductility, and residual stress across the coatings.

As can be observed from Figure 4, the thickness of (Ni,Pt)Al phase is greater than $PtAl_2$+(Ni,Pt)Al and IDZ. Based on the report by Alam *et al.* [26], the stoichiometry and the resultant defect structure of the (Ni,Pt)Al phase affect its strength specifications. Under LTHA, the coating composition is hyper-stoichiometric (Al-rich), and under HTLA the composition is hypo-stoichiometric (Ni-rich) (Fig. 7). Vacancy defects are more evident in the hyper-stoichiometric composition, while substitution defects are dominant in the hypo-stoichiometric. Coating hardness property is affected by the change in stoichiometry. Vacancy defects in hyper-stoichiometric create greater hardness than substitution defects in hypo-stoichiometric. In this research, the micro-hardness test was performed across the coatings and the test results showed hardness values in the ranges of 970-1004 and 820-872 Vickers under LTHA and HTLA, respectively. It has been reported that (Ni,Pt)Al phase is accumulated around vacancy defects more than around a substitution defects. In addition, there is a strain field around the vacancy defects. These two factors contribute to increased coating strength under LTHA [26].

Another reason for more decline of the fatigue life in HTLA compared to LTHA, despite its smaller thickness than LTHA, is the diffusion of elements from the coatings to the substrate (and vice versa) and the formation of intermetallic phases. Some of the undesired phases are formed across the coating–substrate interface (IDZ). Referring to Figure 4, it is observed that the thickness of the IDZ layer is smaller in LTHA. Chromium is one of the elements that is present in this layer. The increment in the chromium content will result in the formation of TCP phases [20]. Figure 6 shows that the percentage of this element in IDZ is higher under HTLA, so the formation of $Cr_{61}Co_{39}$ (the σ phase) [20] is more likely.

Moreover, for LTHA, this is aluminum that diffused to the base metal; while in HTLA, nickel would be diffused from base to coating and the base alloy would become poor in nickel. Nickel is one of the main elements of γ' phase, so the reduction of nickel in this

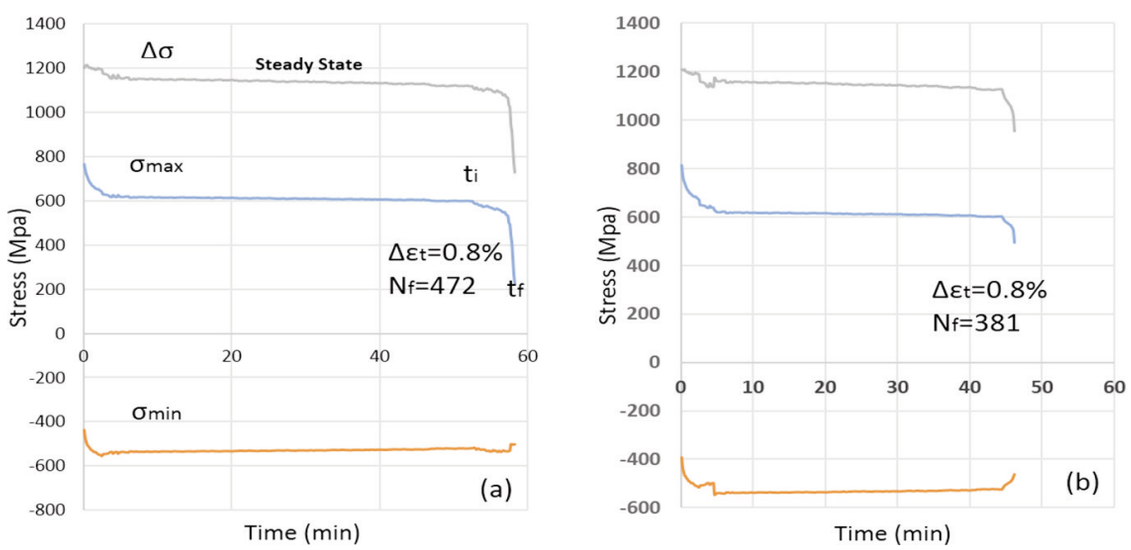

Figure 13. *Variations of maximum and minimum stresses with time for coated specimens under LTHA condition at total strain of 0.8%, temperature of 871ºC, and initial platinum layer thicknesses of (a) 2μm, and (b) 8μm*

phase and depletion of γ′ phase subsequently near the outer surface will be accompanied by the reduction of base alloy strength in HTLA.

Residual stress was also measured in two conditions of HTLA and LTHA for specimens with the initial platinum layer thickness of 8µm by XRD technique. Accordingly, the elastic strain of the coatings applied under LTHA and HTLA were found to be 1.39×10^{-3} and 2.01×10^{-3}, respectively. By consideration of coating elastic modulus (110 GPa) [26] and the application of Hook's Law ($\sigma = E\mathcal{E}$), the value of the residual stresses was calculated as 160 and 221 MPa, for LTHA and HTLA, respectively. As can be observed, the value of tensile residual stress was higher under HTLA, presenting another reason behind the further decrease in the fatigue life under HTLA. Watanabe *et al.* [27] calculated residual stress in a single phase Pt-Al coating, equal to 140 MPa.

3.2.5. Fatigue life calculation

Hysteresis loops are also used for the determination of the fatigue life coefficients values for the uncoated and coated specimens.

The equation for the stable hysteresis loop curve can be written as Eq. (1), where K' and n' are cyclic strength coefficient and cyclic strain hardening exponent, respectively, $\Delta\varepsilon$ is the strain range and $\Delta\sigma$ is the stress range [28].

$$\Delta\varepsilon = \left(\frac{\Delta\sigma}{E}\right) + 2\left(\frac{\Delta\sigma}{2K'}\right)^{\frac{1}{n'}} \quad (1)$$

The coefficients K' and n' can be calculated via linear regression analysis and fitting the logarithmic curve of Eq. (2) to the data obtained from fatigue tests [5], where σ_a and ε_{ap} is stress amplitude and plastic strain amplitude. The values of these parameters for the uncoated (Fig. 14a) and coated (Fig. 15a and 16a) specimens with 2µm and 8µm of platinum under HTLA and LTHA are reported in Table 7.

$$\log\sigma_a = \log K' + n' \log\varepsilon_{ap} \quad (2)$$

As is evident from the data reported in Table 7, the peak values of K'=1774.18 MPa and n'=0.1702 are related to the uncoated specimen, while the corresponding values to the coated specimens under either of the aluminizing conditions followed a decreasing trend with increasing the platinum thickness, reaching a minimum for the coated specimen under HTLA with 8µm of platinum (K'=1505.56 MPa and n' = 0.1329).

The fatigue life of a part can be estimated using

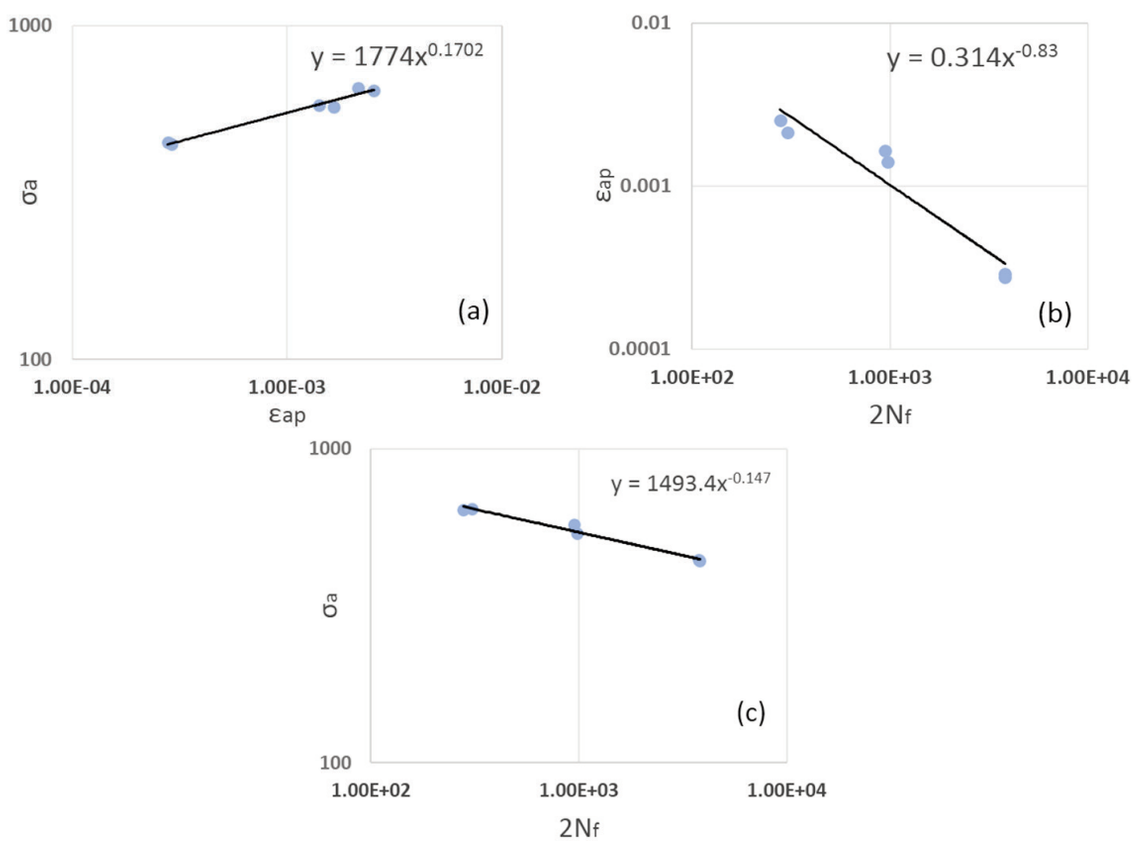

Figure 14. *(a) Cyclic stress-strain, (b) Coffin-Manson's, and (c) Basquin's plots for uncoated alloy Rene®80*

various methods. Coffin-Manson methodology, Eq. (3), is one of the most common approaches to the estimation of the fatigue life [21, 22].

$$\frac{\Delta\varepsilon_t}{2}=\frac{\Delta\varepsilon_e}{2}+\frac{\Delta\varepsilon_p}{2}=\frac{\sigma_f^{'}}{E}\left(2N_f\right)^b+\varepsilon_f^{'}\left(2N_f\right)^c \quad (3)$$

Where $\Delta\varepsilon_t$ is total strain, E is elastic modulus, N_f is the final number of cycles. Fatigue parameters in the above relationship include σ'_f (fatigue strength coefficient), b (fatigue strength exponent), ε'_f (fatigue ductility coefficient), and c (fatigue ductility exponent).

In order to determine the parameters c, ε'_f, b, and σ'_f, the curves expressed in Eq. (4) (Coffin-Manson plot) and Eq. (5) (Basquin plot) were drawn on logarithmic scale based on the data obtained from the fatigue tests, followed by plotting the hysteresis loops and nonlinear regression analysis [5]. The values of these parameters are reported in Table 7.

$$\log\varepsilon_{ap}=\log\varepsilon'_f+c\,\log\left(2N_f\right) \quad (4)$$

$$\log\sigma_a=\log\sigma'_f+b\,\log\left(2N_f\right) \quad (5)$$

The plots of versus $2N_f$ (Eq. (4)) and versus $2N_f$ (Eq. (5)) for the uncoated specimen are presented in Figures 14b and 14c. The corresponding plots to the coated specimens with 2µm and 8µm of platinum under LTHA and HTLA are shown in Figures 15b, c, and 16b, c.

As can be observed, although the application of the platinum-aluminide coatings under either of the aluminizing conditions and with 2µm and 8µm thickness of platinum lead to a decrease in fatigue life of the alloy Rene®80, as is evident on the plots presented in Figures 15b, c and 16b, c, this decrease is more significant on the Coffin-Manson plot than on the Basquin plot, which determines the alloy resistance to plastic strain. Given that the second part of Eq. (3) is significantly larger than its first part in LCF, so the design calculations under LCF are based on strain control, while for high cycle fatigue design calculations the first part of the equation is larger and stress control is considered.

3.2.6. Fractography

At first, fatigue fracture surface was observed in the substrate of the uncoated and coated specimens. Figure 17 shows the surface of the uncoated specimen of the alloy Rene®80 after fatigue failure at 871ºc and $\Delta\varepsilon_t$ = 0.8%.

In Figure 17a, the fatigue fracture surface includes the fatigue initiation zone (A), fatigue crack growth zone (B), and ultimate zone of rapid failure (C) [29]. Performing tests at elevated temperature results in the surface oxidation of the uncoated alloy, and these points provide suitable sites for fatigue crack nucleation. Because of the diffusion of Al into the surface due to oxidation (Al_2O_3- according to XRD results (Fig. 18)), γ′ phase will be poor in this element. Due to the depletion of the near-surface area from γ′, the alloy strength decreases, providing a basis for micro-crack nucleation. No difference was seen between the coated and the uncoated substrate.

Rapid and frequent formation of the oxidation layer on the crack tips has an effect on the growth rate of the cracks. The oxidation layer developed in the crack tip is much more brittle than the alloy surrounding the crack, so it is easily broken. In the next stage, following the breakage of the oxidation layer upon the application of cyclic stress, the alloy is exposed to air and hence re-oxidized, smoothing the way for further crack growth until the final failure. On the other hand, given that grain boundaries of poly-crystalline alloys are among the latest areas developed during the solidification process, melt impurities are commonly concentrated in these zones, making the zones weaker (casting defects). Therefore, under cyclic loading grain boundaries on the oxidized surface of the alloy serve as a source for nucleation and the growth of fatigue cracks. As observed in Figure 17b, under the effect of cyclic stress, cracks have been developed along the boundaries of the surface grains. As shown in Figure 19a, fatigue fracture surface includes cleavage (brittle fracture), dimples (ductile failure), and grain boundary cracks. Figure 19b shows brittle and ductile fracture surface at higher magnification.

The dimples are a result of the disintegration of the carbides-matrix interface upon the application of

***Table 7**. Coefficients of cyclic stress-strain for the Coffin-Manson and Basquin plots for uncoated and coated specimens with different thicknesses of platinum under HTLA and LTHA*

Coefficients			K'(Mpa)	n′	ε'_f	c	σ'_f (Mpa)	b
uncoated			1774.18	0.1702	0.314	-0.8296	1493.4	-0.1469
HTLA	Pt thickness	2	1717.11	0.1613	0.173	-0.7664	1352.38	-0.1301
		8	1505.56	0.1329	0.07	-0.7082	1104.84	-0.1016
LTHA		2	1740.2	0.1649	0.235	-0.8003	1439.46	-0.1391
		8	1646.26	0.1484	0.0924	-0.7138	1233.38	-0.1158

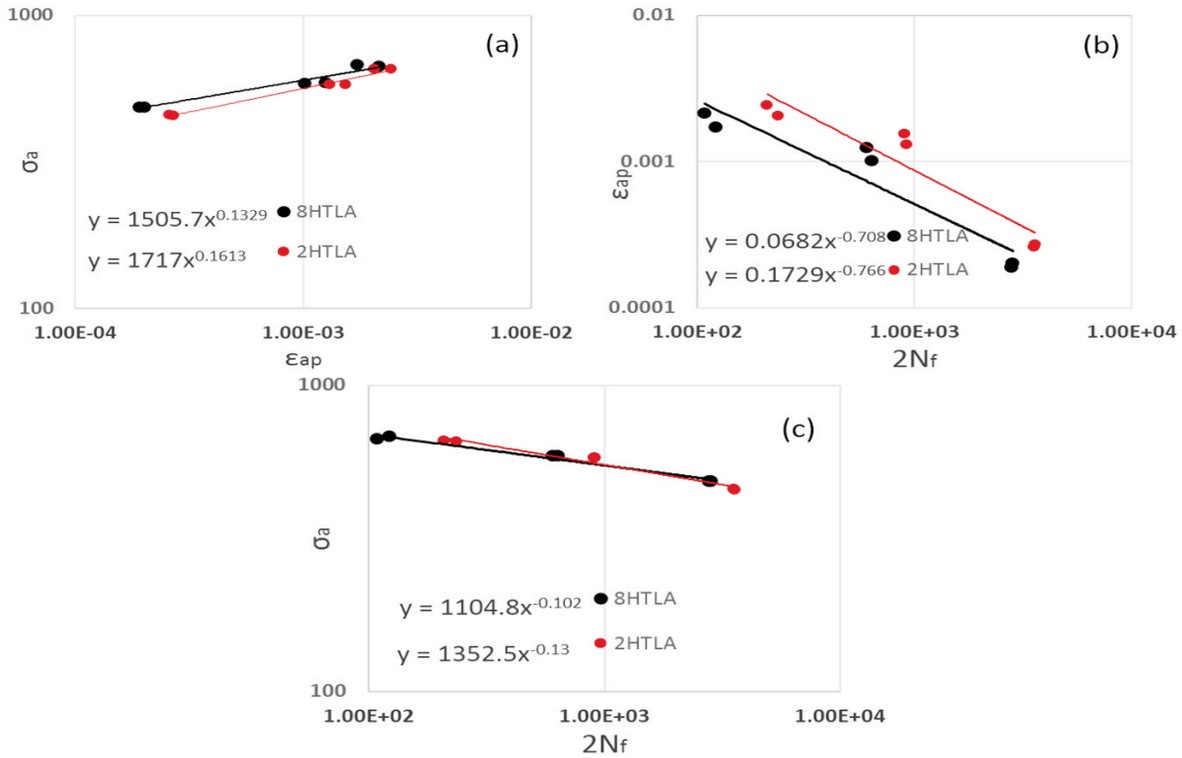

Figure 15 *Comparison between plots of (a) cyclic stress-strain, (b) Coffin-Manson's, and (c) Basquin's plots for coated specimens with 2 and 8μm of platinum under HTLA condition*

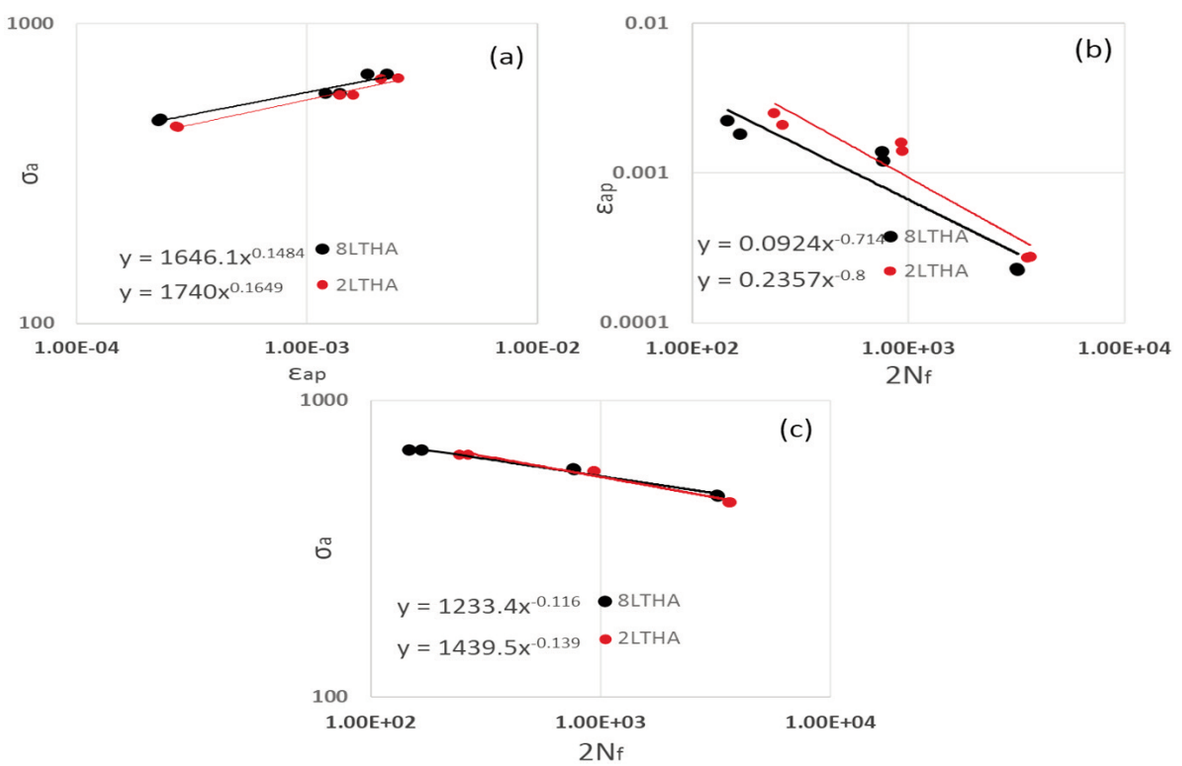

Figure 16. *Comparison between plots of (a) cyclic stress-strain, (b) Coffin-Manson, and (c) Basquin plots for coated specimens with 2 μm and 8μm of platinum under LTHA condition*

plastic strain, and the resultant plastic deformation of the surface. Results of EDS (Fig. 19c) analysis at point A (Fig. 19a) confirmed the presence of TiC carbide within the dimples. The observation of both brittle and ductile failure zones at the same time is an indication of a mixed mode for alloy Rene®80 specimens under LCF test at 871°C.

Figure 20 shows a longitudinal view of the fracture surface of the uncoated alloy as well as those of coated alloys with 2µm and 8µm of platinum via aluminizing under HTLA and LTHA at the total strain of $\Delta\varepsilon t = 0.8\%$ and temperature of 871°C. In all of the specimens, the cracks were seen to be nucleated on the alloy surface under the effects of cyclic loads. As observed, in the uncoated specimen, the crack with thick tip is nucleated on the alloy surface from the oxidized layer and grew in the perpendicular direction to the direction of applied stress. However, thanks to appropriate ductility of the alloy, the length of cracks has remained within the range of 25-28µm in some cases. In the coated specimens with 2µm and 8µm of platinum under HTLA, the crack nucleation started from the bi-phase zone of the coating on the alloy surface and grew in the perpendicular direction to the

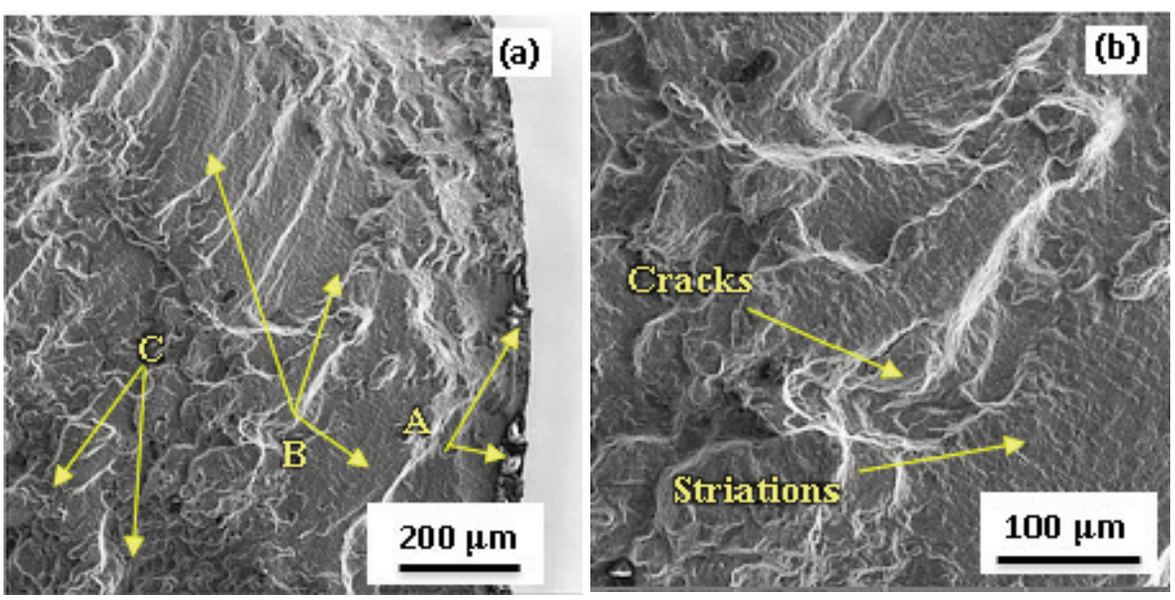

Figure 17. *SEM image of (a) fatigue fracture surface of the uncoated specimen at T = 871°C, R = 0, and Δεt = 0.8%, and (b) fatigue crack growth zone (B) at higher magnification*

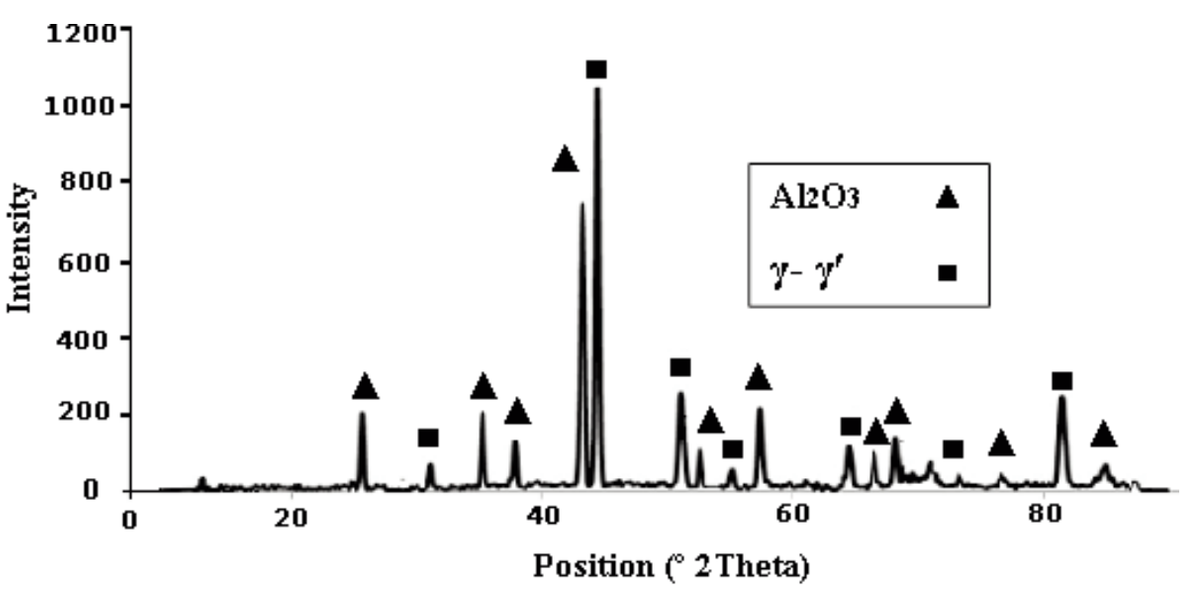

Figure 18. *Result of XRD -Surface of uncoated sample*

direction of applied stress within (Ni, Pt)Al zone, and entered the substrate once passed through IDZ zone. In both the thicknesses of platinum in this aluminizing condition, the crack length was longer than the coating thicknesses and grew by125µm and 131µm, respectively. The crack was thicker when the initial platinum thickness was 8µm.

However, with the platinum thickness of 2µm and under the LTHA, the crack was observed to nucleate from the surface and grow in the direction of applied stress at an oblique angle to an extent equal to the coating thickness, but it did not pass beyond IDZ zone. This was not the case for the 8µm-thick platinum coating under the same condition, where the cracks grew beyond IDZ zone into the substrate along a total growth length of 156µm.The important point to note is the sharpness of the crack tip in all of the coated specimens, as compared to the uncoated specimen, indicating further stress concentration at the crack tip.

The development of crack on the surface in both of the coating conditions (HTLA/LTHA) and its growth throughout the entire coating indicated the brittleness of the platinum-aluminide coating, its susceptibility to crack nucleation, and the closeness of the test temperature (871°C) to DBTT of the coating. As such, the coating cannot retard the crack growth within itself. The crack growth termination in the LTHA with an initial platinum thickness of 2µm within IDZ zone and its growth into the substrate in other conditions

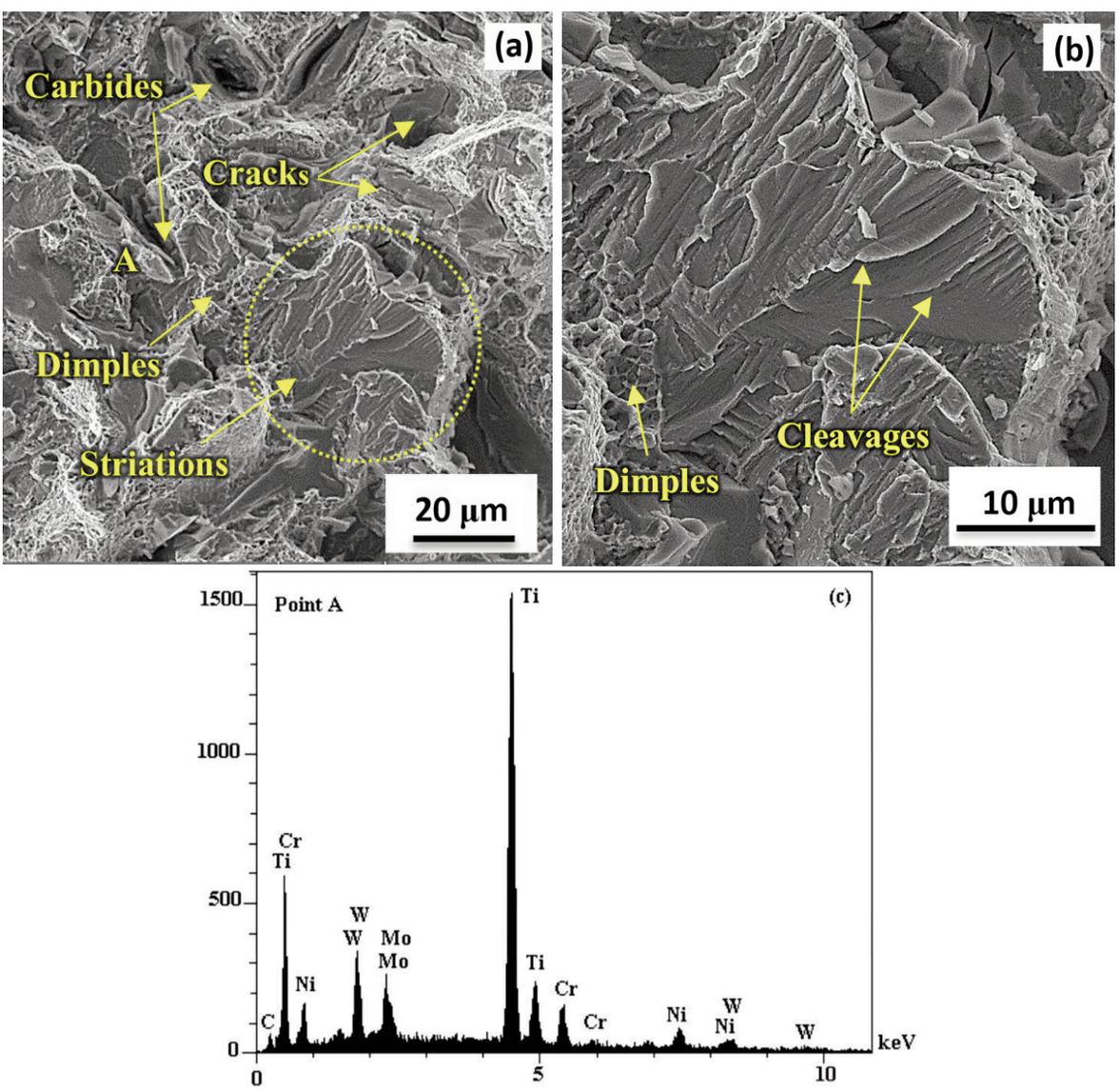

Figure 19. *SEM image of (a) fatigue fracture surface of the uncoated specimen at T = 871°C, R = 0, and εΔt = 0.8%, (b) fatigue fracture surface at higher magnification, and (c) EDS analysis result*

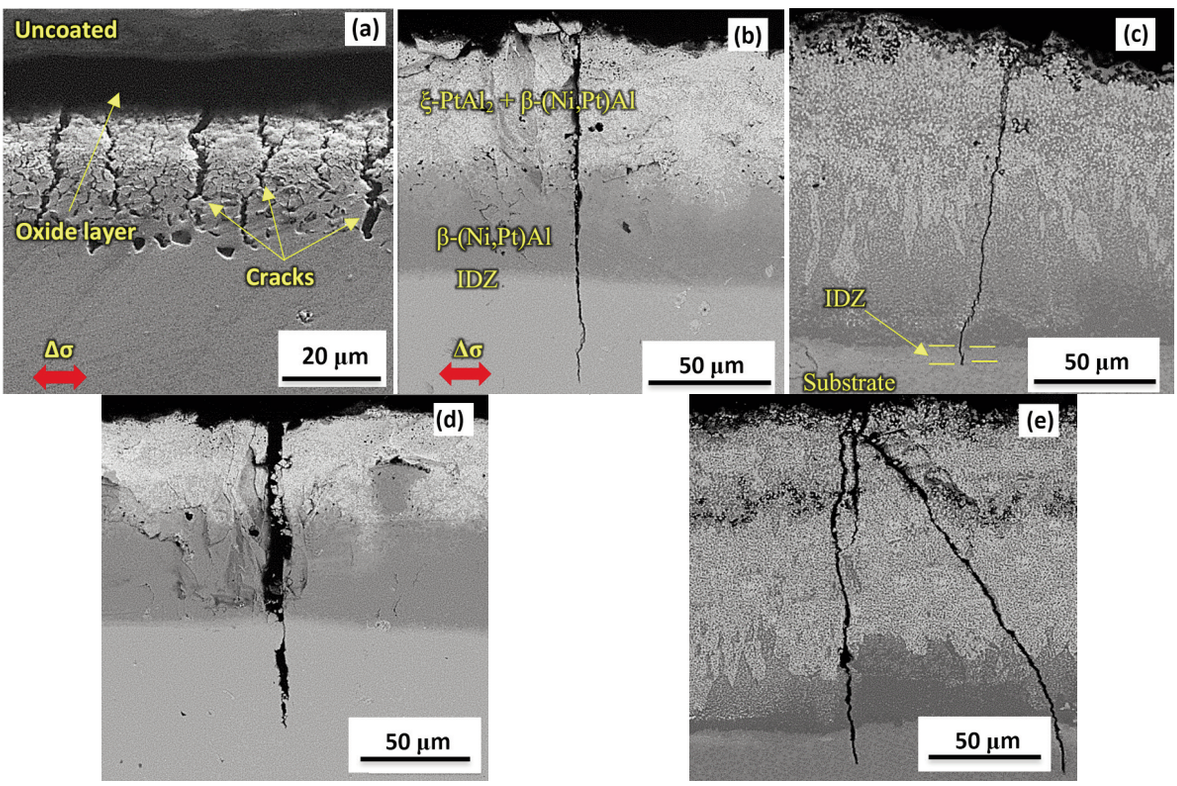

Figure 20. *SEM images of longitudinal cross-section of the failed fatigue specimens: (a) uncoated and coated specimens with (b) 2µm of platinum under HTLA, (c) 2µm of platinum under LTHA, (d) 8µm of platinum under HTLA, and (e) 8µm of platinum under LTHA, at T = 871°C, R = 0, and* $\Delta\varepsilon_t$ *= 0.8%*

can be attributed to the ductility of the coated alloy. As can be observed in Table 4, the smallest drop in ductility with reference to the uncoated case, was that of the coated specimen with 2µm of platinum via LTHA, where 12.8% and 4.3% decreases were found to be related to %EL and %RA, respectively. Therefore, despite the crack growth into the coating, sufficient ductility of the alloy prevented the crack from growing into the base alloy. In Table 3, where tensile properties of the uncoated alloy are presented, %EL and %RA of the uncoated specimen were measured to be 8 and 16% (in average), respectively, which are higher than all of the coating approaches.

4. Conclusions

In all cases, the coatings were made from a three-layer structure including a bi-phase external layer $PtAl_2$+(Ni,Pt)Al, a single-phase intermediate layer (Ni,Pt)Al , and coating-substrate interface layer IDZ.

The presence of platinum-aluminide coatings decreases tensile strength and ductility of alloy Rene®80. This reduction is more considerable in HTLA compared to LTHA.

Low cycle fatigue life is reduced in the coated specimens as compared to the uncoated one. This reduction is more significant in HTLA with 8µm of the platinum layer. For this coating, at total strains of 0.4, 0.8, and 1.2%, this reduction is determined 26%,

35%, and 59.5%, compared to the uncoated specimen, respectively. While this reduction is determined 3.5%, 4.5%, and 13% in LTHA with 2µm of the platinum layer at the same total strains, respectively.

Fracture surface analysis shows a mixed mode of ductile and brittle failure under cyclic loading in both uncoated and coated specimens. In the uncoated specimen, the crack initiated from the oxidized layer and in coated specimens, the crack initiated from coatings, respectively, and diffused into the base alloy. The crack remained within the coating only in the case with an initial platinum layer thickness of 2µm and LTHA condition.

References

[1] M. Lavella, Metals, 159 (2016) 1-15.
[2] R. Strife, J. Phys. IV., 3 (1993) 17-42.
[3] G.R. Krishna, D.K. Das, V. Singh, S.V Joshi, Mater. Sci. Eng. A., 251 (1998) 40-47.
[4] K. Rahmani, S. Nategh, Mater. Sci. Eng. A., 486 (2008) 686-695.

[5] M. Julis, K. Obrtlik, S. Pospisilova, T. Podrabsky, J. Polaka, Procedia Eng., 2 (2010) 1983–1989.

[6] M. Mansuri, S.S.M. Hadavi, E. Zare, Metal. Mater. Trans. A., 47 (2016) 293-300.

[7] K. Yuan, Appl. Mech. Mater., 148 (2012) 24-29.

[8] ASTM E606/E606M-12, Standard Test Method for Strain-Controlled Fatigue Testing, (2012) 1-16.

[9] ASTM E1417/E1417/M-13, Standard Practice for Liquid Penetrant Testing, (2013) 1-11.

[10] ASTM E1742/E1742-12, Standard Practice for Radiographic Examination, (2012) 1-17.

[11] AMS 5403 A, Specification for alloy casting, investment, corrosion and heat resistant, 1995.

[12] I. Rose and C. Whittington, Nickel plating handbook, Nickel Institute, Brussels, 2014 p. 15.

[13] M. Yavorska, J. Sieniawski, Arch. Mater. Sci. Eng., 45 (2010) 56-60.

[14] K. Shirvani, S. Firouzi, A. Rashidghamat, Corros. Sci., 55 (2012) 378-384.

[15] ASTM E3-11, Standard Guide for Preparation of Metallographic Samples, (2011) 1-12.

[16] ASTM E883-11, Standard Guide for Reflected–Light Photomicrography, (2011) 1-16.

[17] ASTM) E 384- 99, Standard Test Method for Microindentation Hardness of Materials, (1999) 1-24.

[18] ASTM E 21-09, Standard Test Methods for Elevated Temperature Tension Tests of Metallic Materials, (2009) 1-8.

[19] D.K. Das, V. Singh, S. Vakil, Metall. Mater. Trans. A., 31(8) (2000) 2037-2047.

[20] K. Yuan, [dissertation]. Linköping University, Sweden, 2013.

[21] J.A. Bannantine, J.J. Comer, J.L. Handrock, Fundamentals of Metal Fatigue Analysis. Englewood Cliffs, New Jersey, 1990, p.48.

[22] K. Rahmani, S. Nategh, Mater. Sci. Eng. A., 494 (2008) 385-390.

[23] X. Jianping, X. Jiyuan, The American Society of mechanical engineers, (1985) 1-7.

[24] M.Z. Alam, B. Srivathsa, S.V. Kamat, Trans. Indian. Inst. Met., 64 (2011) 57-61.

[25] H.J. Kolkman, Mater. Sci. Eng. A., 89 (1987) 81-91.

[26] M.Z. Alam, S.V. Kamat, V. Jayaram, D.K. DAS, Acta Mater. 61 (2013) 1093-1105.

[27] M. Watanabe, D.R. Mumm, S. Chiras, A.G. Evans, Scripta Mater. 46 (2001) 67-70.

[28] R. Stephens, A. Fatemi, R.R. Stephens, Metal Fatigue in Engineering. 2nd ed. A Wiley-interscience publication, New Jersey, 1980, p.105.

[29] P. Zhang, Z. Qiang, C. Gang, H. Qin, C. Wang, Mater. J., 8 (2015) 6179-6194.

UTICAJ OSOBINA PLATINSKOG ALUMINIDA KAO PREMAZA NA IZDRŽLJIVOST SUPER LEGURE NA BAZI NIKLA RENE®80 NA VISOKIM TEMPERATURAMA

M.M. Barjesteh [a], K. Zangeneh-Madar [a,*], S.M. Abbasi [a], K. Shirvani [b]

[a*] Univerzitet za tehnologiju Malek Aštar (MUT), Istraživački centar za metalne materijale, Teheran, Iran
[b] Iranska istraživačka organizacija za nauku i tehnologiju (IROST), Odsek za napredne materijale I nove energije, Teheran, Iran

Apstract

Niskociklični zamor je najvažniji režim kvara kod rotacionog motora turbine u avijaciji/industriji. U ovom radu se istražuje uticaj koji parametari Pt-aluminid premaza imaju na niskociklični zamor pri visokim temperaturama na super leguru Rene®80 koja se koristi za izradu lopatica turbina. U tu svrhu su uzorci za ispitivanje zamora materijala na početku premazani slojevima platine različitih debljina (2µm i 8µm). Zatim je izvršen proces aluminizacije pri uslovima niske temperature-visoke aktivnosti i visoke temperature-niske aktivnosti. Rezultati ispitivanja mikrostrukture izvedeni su uz pomoć elektronskog skenirajućeg mikroskopa i fazna analiza izvedena uz pomoć rendgenske difrakcije pokazala je troslojnu strukturu premaza (bifazna (Ni,Pt)Al+$PtAl_2$, jednofazna (Ni,Pt)Al, i interdifuziona zona) različitog hemijskog sastava obe debljine sloja platine uz korišćenje oba metoda aluminizacije. Takođe, rezultati testova niskocikličnog zamora pri 871 °C, R=0 i pri stopi deformacije od 2×10^{-3} s^{-1} pokazali su pad osobina zamora u uzorcima koji su imali premaz u poređenju sa uzorkom koji nije imao premaz, pri ukupnim naporima od 0.4, 0.8, i 1.2%. Ovo umanjenje je bilo niže pri uslovima niske temperature-visoke aktivnosti i slojem platine debljine 2µm, dok je pri uslovima visoke temperature-niske aktivnosti i slojem platine od 8µm bilo značajnije. Fraktografsko ispitivanje uzoraka sa i bez premaza ukazalo je na mešoviti oblik duktilne i krhke frakture.

Ključne reči: *Superalloy; Rene®80; platinum-aluminide; low cycle fatigue; fractography*